Supporting Information

In-situ evolution of bulk-active γ-CoOOH with immobilized Gd dopants enabling an efficient oxygen evolution electrocatalysis

Tianjue Hou, Ruotao Yang, Jiaxin Xu, Xiaodie He, Hongyuan Yang, Prashanth W. Menezes and Ziliang Chen**

Figures

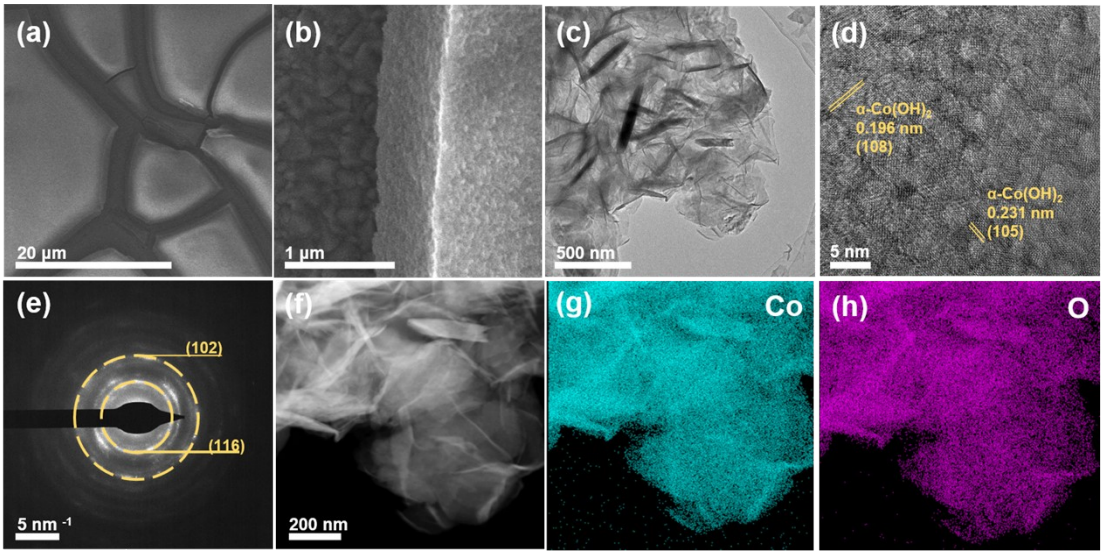

Fig. S1. (a, b) The FESEM images of α-$Co(OH)_2$/FTO. (c) The TEM images, (d) HRTEM image, and (e) SAED pattern together with the corresponding (f) HAADF pattern as well as the elemental mapping of (g) Co and (h) O for the α-$Co(OH)_2$ peeled from the FTO substrate.

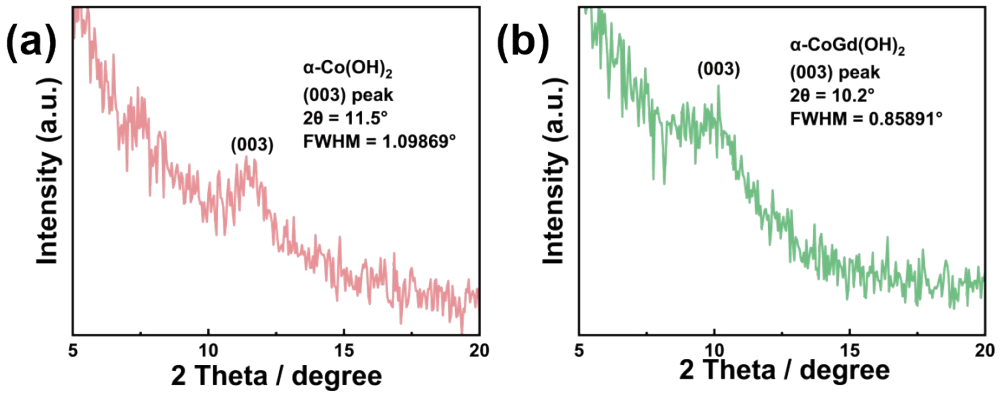

Fig. S2. The XRD patterns with 2 theta values below 10° for α-$Co(OH)_2$ and α-$CoGd(OH)_2$ together with the full width at half maximum (FWHM) analysis on their respective (003) peak.

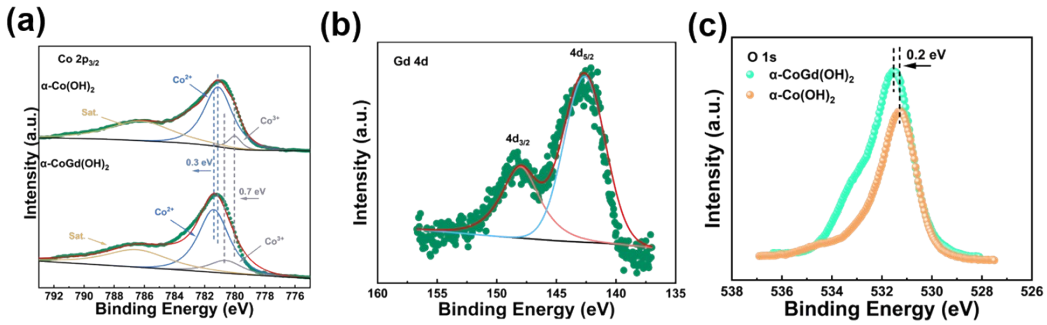

Fig. S3. The XPS spectra of (a) Co $2p_{3/2}$ for α-$CoGd(OH)_2$/FTO and α-$Co(OH)_2$/FTO, (b) Gd 4d for α-$CoGd(OH)_2$/FTO, as well as (c) O 1s for α-$CoGd(OH)_2$/FTO and α-$Co(OH)_2$/FTO, respectively.

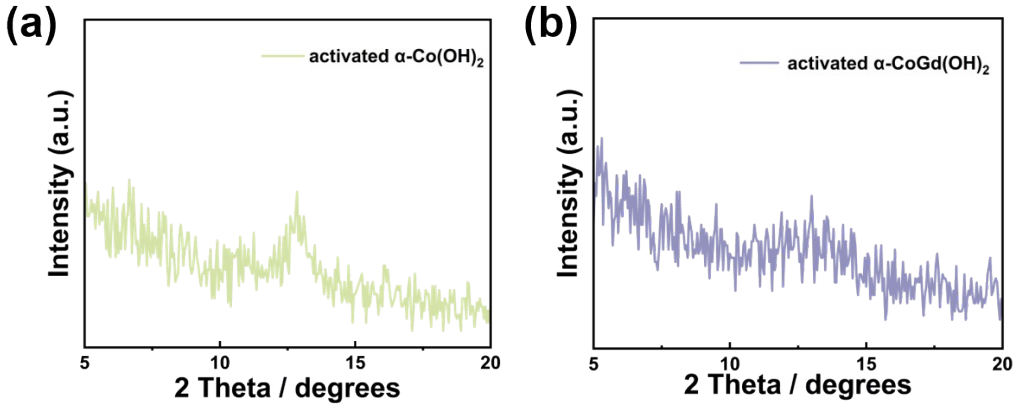

Fig. S4. The powder XRD patterns of the activated α-$Co(OH)_2$ and α-$CoGd(OH)_2$, respectively, recorded using the Grazing incidence (GI) mode. Note that the beam-knife was also employed to minimize air scattering at the low 2 theta region.

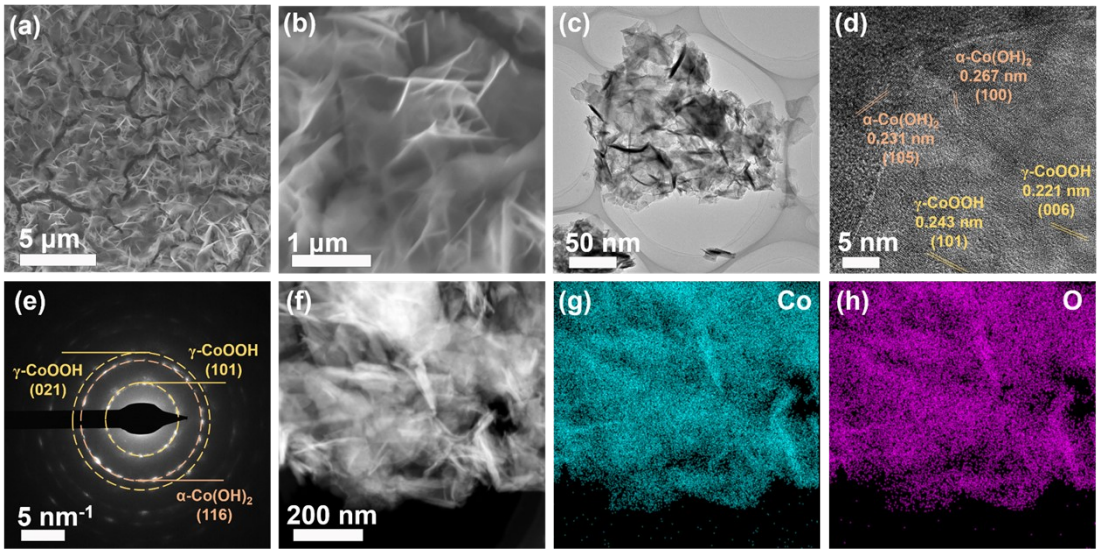

Fig. S5. (a, b) The FESEM images of α-$Co(OH)_2$/FTO after activation. (c) The TEM images, (d) HRTEM image, and (e) SAED pattern together with the corresponding (f) HAADF pattern as well as the elemental mapping of (g) Co and (h) O for the α-$Co(OH)_2$ after activation (peeled from the FTO substrate).

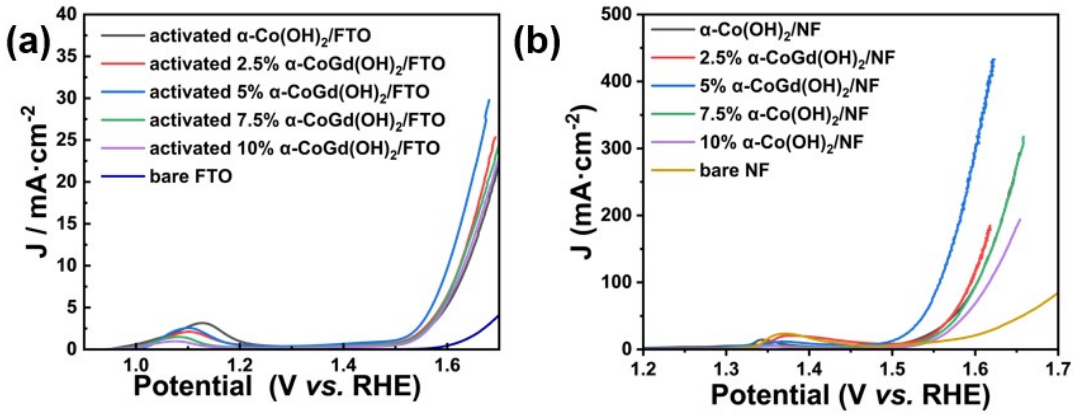

Fig. S6. The LSV curves of (a) the FTO- and (b) NF-supported 2.5% α-CoGd$(OH)_2$, 5% α-CoGd$(OH)_2$, 7.5% α-CoGd$(OH)_2$, and 10% α-CoGd$(OH)_2$. Herein, α-Co$(OH)_2$ was incorporated with different amounts of Gd, which was prepared by adjusting the molar ratio between Co and Gd sources, ranging from 0.975 : 0.025, 0.95 : 0.05, 0.925 : 0.075, to 0.9 : 0.1. Note that the (a) bare FTO and (b) NF, as well as the bare α-Co$(OH)_2$ deposited on (a) FTO and (b) NF were also included. The LSV curves of all the samples were recorded after 20 CV activations.

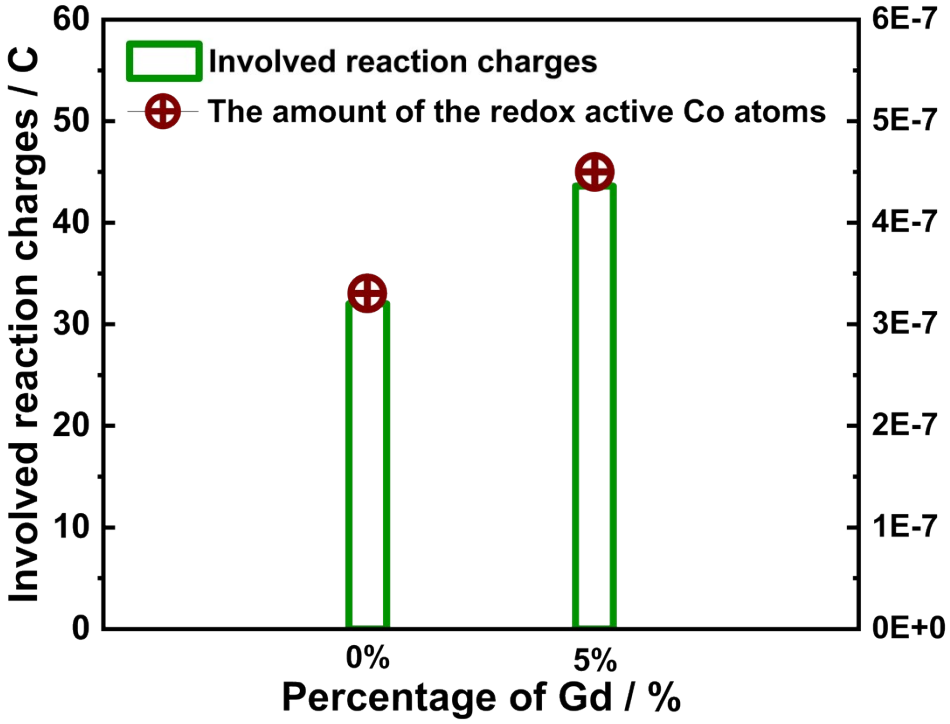

Fig. S7. The correlation between the solution ratio of chemical deposition and the number of active sites. The integration of reduction peaks of α-$Co(OH)_2$ and α-$CoGd(OH)_2$ in the same potential region for the calculation of the amount of electroactive Co atoms. The observed reduction peak can be attributed to the conversion of Co^{3+} ions into Co^{2+} ions, whose area for α-$Co(OH)_2$ and α-$CoGd(OH)_2$ were 0.16011 mV·A cm^{-1} and 0.21805 mV·A cm^{-1}, respectively, as shown in Fig. 5c. Therefore, the involved reaction charge for α-$Co(OH)_2$ and α-$CoGd(OH)_2$ can be calculated through the equation: involved reaction charges (C) = integrated area of reduction peak (V A) / scan rate (V s^{-1}). Furthermore, following to the equation: the number of transferred electrons = involved reaction charges (C) / charge of an electron (1.602×10^{-19} C), The number of the transferred electrons for α-$Co(OH)_2$ and α-$CoGd(OH)_2$ can be determined. Since the corresponding process involves a single electron transfer, the number of transferred electrons aligns with the number of active Co atoms, thus enabling us to draw this conclusion.

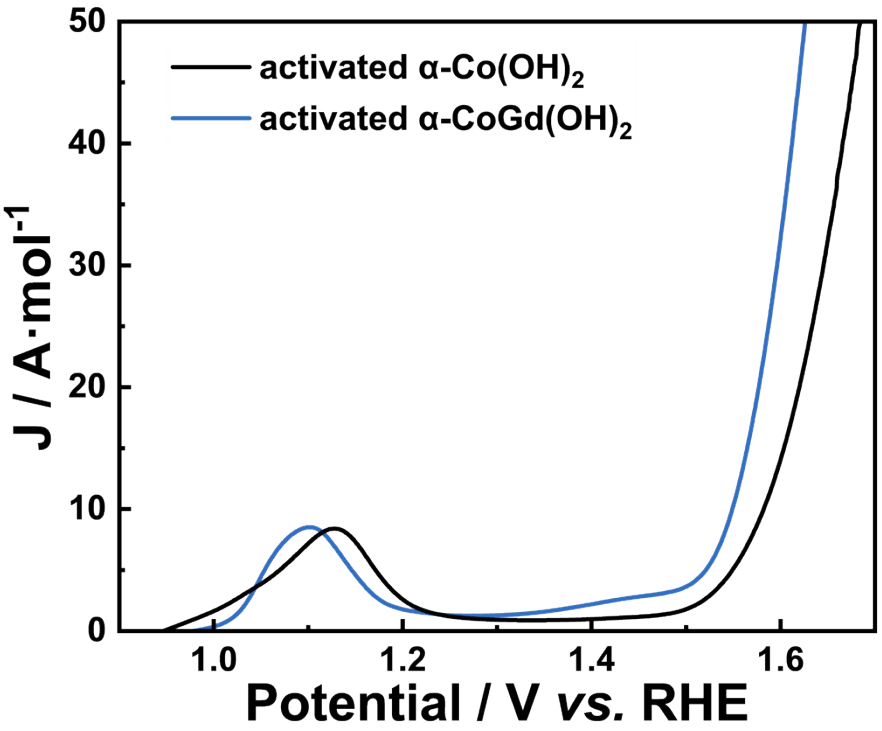

Fig. S8. The current from the LSV data in Fig. 5a of the main text normalized against the number of the redox active Co atoms.

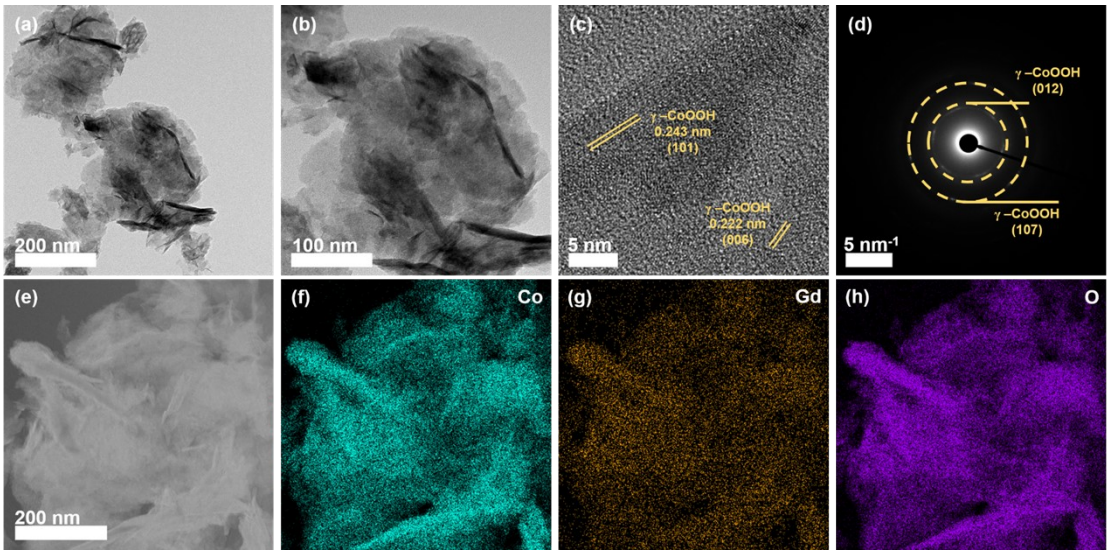

Fig. S9. (a, b) The TEM images, (c) HRTEM image, and (d) SAED pattern together with the corresponding (e) HAADF pattern as well as the elemental mapping of (f) Co, (g) Gd, and (h) O for the activated α-$CoGd(OH)_2$ after 24 h CA at a current density of ~10 mA cm^{-2} (peeled from the FTO substrate).

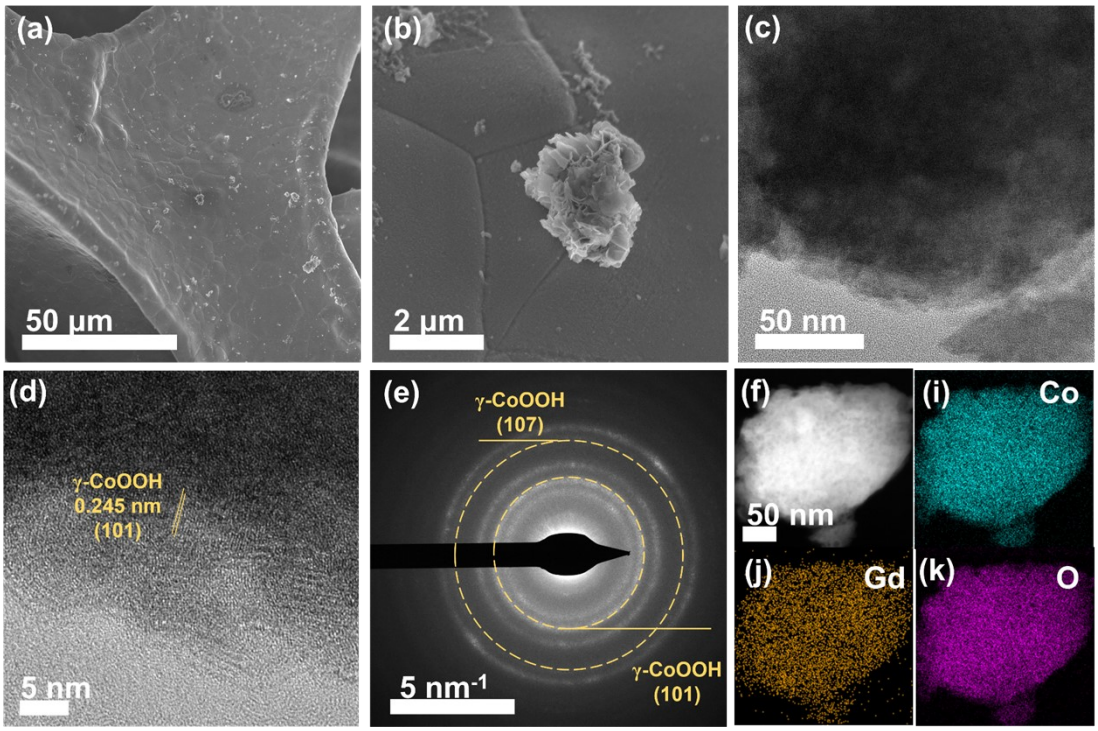

Fig. S10. (a, b) The FESEM images of α-$CoGd(OH)_2$/NF. (c) The TEM images, (d) HRTEM image, and (e) SAED pattern together with the corresponding (f) HAADF pattern as well as the elemental mapping of (g) Co, (h) Gd, and (i) O for the activated α-$CoGd(OH)_2$ peeled from the NF substrate.

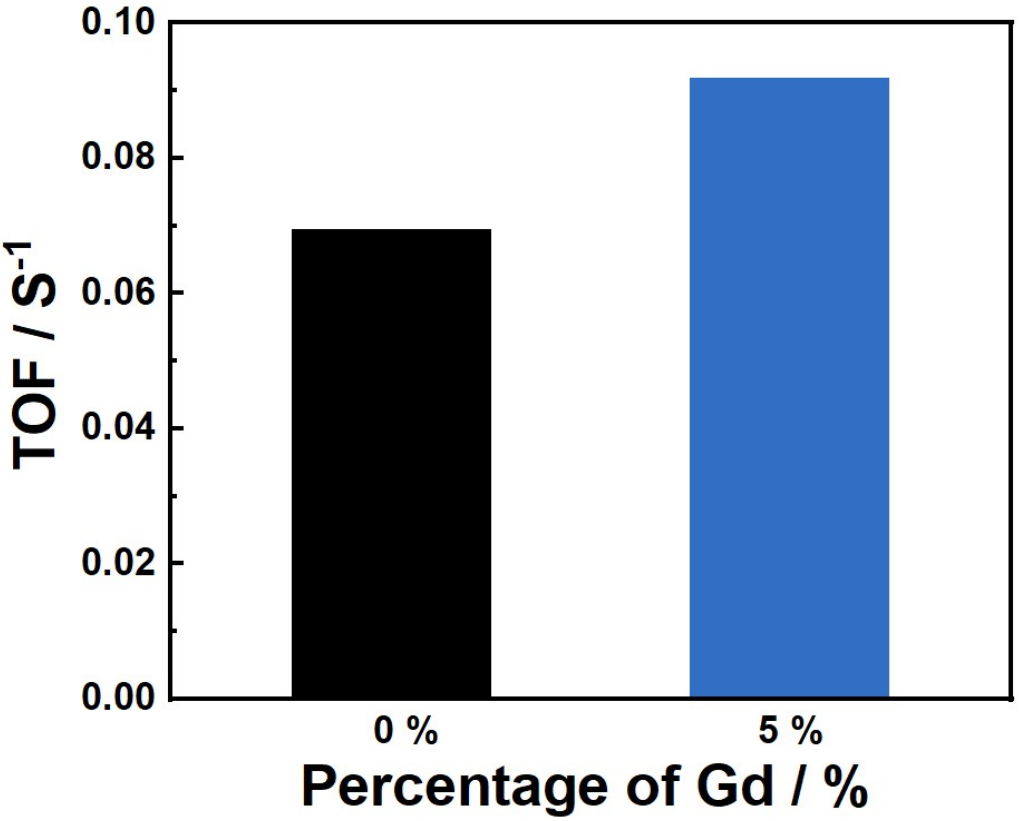

Fig. S11. The turnover frequency (TOF) of activated α-$Co(OH)_2$ and α-$CoGd(OH)_2$ at the overpotential of 400 mV.[1] **TOF = j · N_A / F ·n· Γ** where *j* is the current density, N_A is the Avogadro number, *n* is the number of electrons transferred for the evolution of a single O_2 molecule, *F* is the Faraday constant, and Γ is the surface concentration or the number of active Co sites.

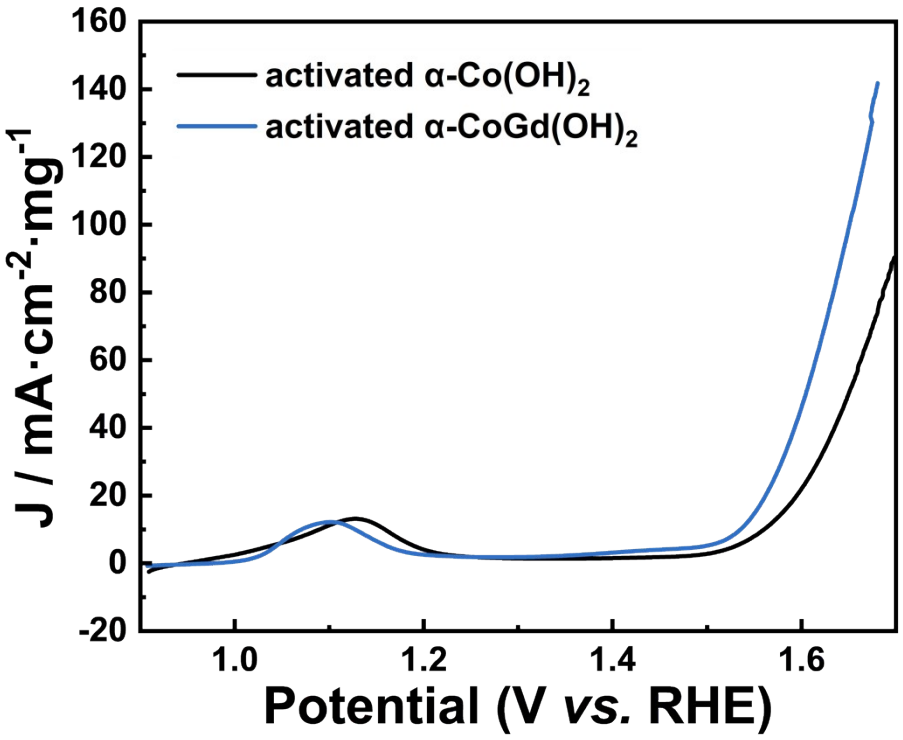

Fig. S12. The current from the LSV data in Fig. 5a of the main text normalized against the mass of the deposited catalyst.[2]

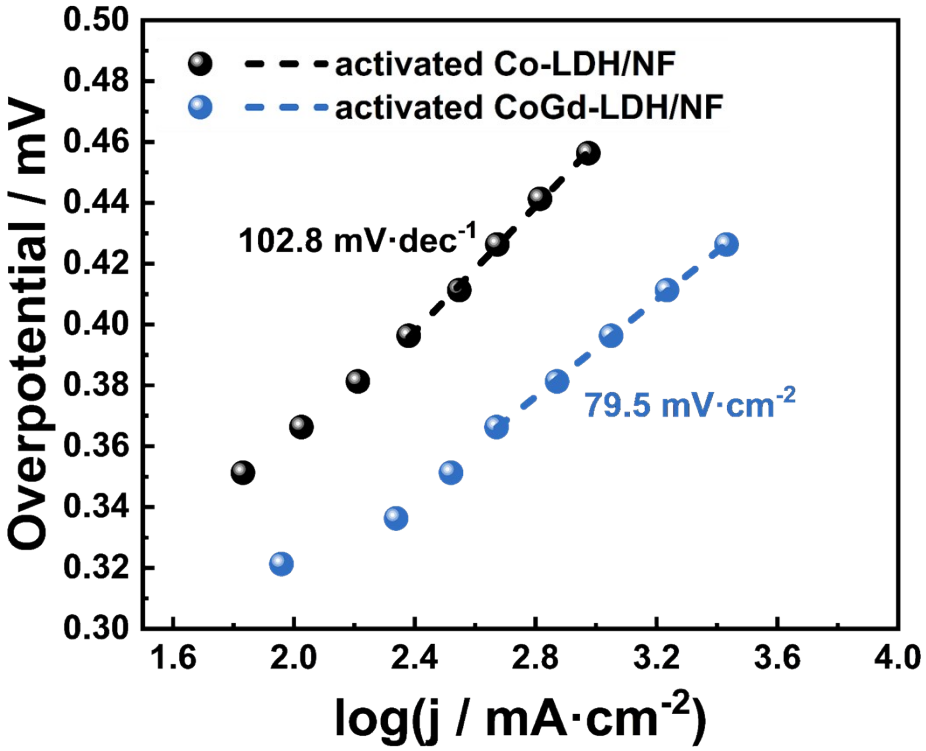

Fig. S13. The Tafel slope plots of the activated α-$CoGd(OH)_2$/NF and α-$Co(OH)_2$/NF determined by the steady-state method.

Tables

Table S1. The atomic ratio of Co and Gd for α-$CoGd(OH)_2$/FTO determined by EDS.

Atomic ratio	**Co**	**Gd**
Fresh samples	11.07	1
After activation	13.27	1
After stability test	13.12	1

Table S2. The atomic ratio of Co and Gd for α-$CoGd(OH)_2$/FTO determined by ICP analysis.

Atomic ratio	**Co**	**Gd**
Fresh samples	11.90	1
After stability test	12.26	1

Table S3. Rct (Ω), Rs (Ω), CPE (F x s(a2-1)) and a2 of the catalysts deposited on FTO and NF obtained from EIS fitting at an anodic polarization potential of 1.6 V (*vs.* RHE) and from EIS fitting at an anodic polarization potential of 1.55 V (*vs.* RHE), respectively.

	Activated α-$Co(OH)_2$/FTO	**Activated α-$CoGd(OH)_2$/FTO**
R_{ct} **(Ω)**	61.05	21.94
R_s **(Ω)**	10.86	12.1
CPE	0.04036	0.06428
a2	0.9261	0.8539

	Activated α-$Co(OH)_2$/NF	**Activated α-$CoGd(OH)_2$/NF**
R_{ct} **(Ω)**	4.523	2.85
R_s **(Ω)**	1.191	1.061
CPE	0.1551	0.3178
a2	0.9209	0.883

Table S4. The overpotential to deliver a current density of ~100 mA cm^{-2} and tafel slope comparison between α-$CoGd(OH)_2$/NF and other recently reported advanced Co-based catalysts supported on NF for alkaline OER.

NiCoS nanorods	370 mV	130 mV·dec^{-1}	3
CoO nanowires	415 mV	72 mV·dec^{-1}	4
Co-P particles	380 mV	51.1 mV·dec^{-1}	5
3D $Co(OH)_2$@NCST	410 mV	72 mV·dec^{-1}	6
NiCoP nanocone	370 mV	116 mV·dec^{-1}	7
Fe-doped (Ni,Mn)Co nanorods	331 mV	67.8 mV·dec^{-1}	8
Fe-Co-Ni-S*x*	409 mV	93 mV·dec^{-1}	9
NiCoP@NC NA	339 mV	70.5 mV·dec^{-1}	10
Mo-doped CoP nanosheet	330 mV	69.1 mV·dec^{-1}	11
N-C inserted NiCo-LDH nanoplates	352 mV @ 50mA·cm^{-1}	80.1mV ·dec^{-1}	12
NiA-Co(OH)2 film	410 mV	82 mV·dec^{-1}	13
spheres like spinel oxide $CoFe_2O_4$	400 mV	78 mV·dec^{-1}	14
$Co_{0.4}(Hatz)_{0.1}(H4bta)_{0.1}$ nanoclusters	311 mV	84 mV·dec^{-1}	15
Ni-Co-S nanosheets	363 mV	86 mV·dec^{-1}	16
branch like NiCoS	410 mV	64.7 mV·dec^{-1}	17
Gd-doped γ-CoOOH nanosheets	327 mV	79.5 mV·dec^{-1}	this work

Reference

1. S. Anantharaj, P. E. Karthik and S. Noda, *Angew. Chem. Int. Ed.*, 2021, **60**, 23051–23067.
2. L. Yu, S. Sun, H. Li and Z. J. Xu, *Funda. Re.*, 2021, **1**, 448–452.
3. K. Yan, X. Shang, Z. Li, B. Dong, J. Chi, Y. Liu, W. Gao, Y. Chai and C. Liu, *Int. J. Hydrogen Energy*, 2017, **42**, 17129–17135.
4. S. Zhu, J. Lei, L. Zhang and J. He, *In. J. Hydrogen Energy*, 2020, **45**, 8031–8040.
5. Z. Lv, Y. Zhang, K. Wang, T. Yu, X. Liu, G. Wang, G. Xie and L. Jiang, *Mater. Chem. Phys.*, 2019, **235**, 121772.
6. P. Guo, J. Wu, X. Li, J. Luo, W. Lau, H. Liu, X. Sun and L. Liu, *Nano Energy*, 2018, **47**, 96–104.
7. J. Li, G. Wei, Y. Zhu, Y. Xi, X. Pan, Y. Ji, I. V. Zatovsky and W. Han, *J. Mater. Chem. A*, 2017, **5**, 14828–14837.
8. H. Shi, Q. Zha and Y. Ni, *J. Alloys Compd*, 2022, **904**, 164052.
9. S. Zhu, J. Lei, S. Wu, L. Liu, T. Chen, Y. Yuan and C. Ding, *Mater. Lett.*, 2022, **311**, 131549.
10. B. Cao, Y. Cheng, M. Hu, P. Jing, Z. Ma, B. Liu, R. Gao and J. Zhang, *Adv. Funct. Mater.*, 2019, **29**, 1906316.
11. S. Li, L. Bai, H. Shi, X. Hao, L. Chen, X. Qin and G. Shao, *Ionics*, 2021, **27**, 3109–3118.
12. Z. Jia, J. Shang, K. Xue, X. Yang, S. Wang, C. Xu and Q. Wang, *ChemCatChem*, 2023, **15**, e202201469 .
13. K. Patil, P. Babar, D. Lee, V. Karade, E. Jo, S. Korde and J. Kim, *Sustain. Energ. Fuels*, 2020, **4**, 5254-5263
14. S. Zhu, J. Lei, Y. Qin, L. Zhang and L. Lu, *RSC Adv.*, 2019, **9**, 13269–13274.
15. Z. Huang, L. Hao, X. Ma, S. Zhang, R. Zhang, K. Yue and Y. Wang, *Inorg. Chem.*, 2021, **60**, 4047–4057.
16. T. Liu, X. Sun, A. M. Asiri and Y. He, *Int. J. Hydrogen Energy*, 2016, **41**, 7264–7269.
17. Y. Zhang, L. Lin, J. Liu, J. Peng, Z. Chen and L. Chen, *Int. J. Hydrogen Energy*, 2021, **46**, 36629–36639.